Progress in Earth and Planetary Science

RESEARCH ARTICLE Open Access

Spatial accuracy assessment of unmanned aerial vehicle-based structures from motion multi-view stereo photogrammetry for geomorphic observations in initiation zones of debris flows, Ohya landslide, Japan

Haruka Tsunetaka[1*], Norifumi Hotta[2], Yuichi S. Hayakawa[3] and Fumitoshi Imaizumi[4]

Abstract

Fluctuations in sediment storage arising from sediment discharge and recharge in headwater channels are an important factor influencing changes in landforms in mountainous areas, but the frequency of surveys is limited because of access difficulties and complex topography. Although unmanned aerial vehicle-based structure-from-motion photogrammetry (UAV-SfM) may be effective for topographic measurement, its utilization in headwater channels has not been fully examined. We assessed the accuracy and reproducibility of a digital elevation model acquired via UAV-SfM (DEM_{SfM}) in a headwater channel within the Ohya landslide area, Japan, using a DEM acquired via terrestrial laser scanning (DEM_{TLS}). The results indicate that differences in the measured elevation between DEM_{SfM} and DEM_{TLS} in the vicinity of the channel bed ranged from about 0.4 to −0.4 m, with a median of 0.06 m. Hence, the profiles acquired via DEM_{SfM} coincide well with those acquired via DEM_{TLS}, and the spatial distributions and histograms of the measured surface slope were nearly the same for UAV-SfM and TLS. However, part of the DEM_{SfM} indicates low elevation compared with DEM_{TLS}, probably because of topical distortion arising from technical problems in UAV-SfM. The positive and negative differences in volume between DEM_{SfM} and DEM_{TLS} were approximately 200 and −30 m^3, respectively. To remedy this bias, an alignment of the UAV-SfM point cloud using the TLS point cloud in the hillslope sections was conducted, based on an iterative closest point (ICP) algorithm. Consequently, the median of the elevation differences decreased to −0.002 m, resulting in the positive and negative differences becoming approximately 100 m^3. This demonstrates that ICP-based alignment can lead to a reduction of the deviation of differences in the estimated volume. In terms of eliminating biases due to topical distortion in elevation, this approach would be valid for the estimation of volumetric changes using UAV-SfM.

Keywords: UAV-SfM, TLS, ICP, Debris flow

* Correspondence: tsunetakaharuka@ffpri.affrc.go.jp
[1]Forestry and Forest Products Research Institute, 1, Matsunosato, Tsukuba, Ibaraki 305-8687, Japan
Full list of author information is available at the end of the article

Introduction

In headwater channels, sediment production persists for a long time because of weathering promoted by freeze–thaw processes, complex geological features, and steep topography (Imaizumi et al. 2015; Nishii et al. 2018). Such sediments are discharged as torrential flows, e.g., debris flows and debris floods, by heavy rainfall events (Coe et al. 2008; Bel et al. 2017). This fluctuation in sediment storage due to sediment recharge and discharge is related to the sediment cascade system on the watershed scale (Gallo and Lavé 2014). Moreover, the discharge of channel deposits via the descent of torrential flows leads to the process of channelization (McCoy et al. 2013). Therefore, changes in sediment storage in headwater channels are an important factor in geomorphic processes.

Previously, changes in sediment storage have been detected using DEMs acquired via airborne laser scanning (ALS) due to the inaccessibility of headwater channels (Schlunegger et al. 2009; Berger et al. 2011a). Because ALS is an expensive measurement method and radiates lasers from high attitudes, the observation intervals, and spatial resolutions of such DEMs are generally several years and several meters, respectively. Torrential flows often occur several times per year (Coe et al. 2008; Imaizumi et al. 2017), with the result that the characteristics of channel deposits can be spatially and temporally altered within a few months because of the entrainment and deposition of channel deposits (Blasone et al. 2014; Hayakawa et al. 2016). Moreover, changes in the elevation of channel deposits vary widely, from dozens of centimeters to several meters (McCoy et al. 2010, 2012; Berger et al. 2011b; Staley et al. 2011). Therefore, an increase in measurement frequency and spatial resolution is necessary to further examine changes in sediment storage and the distribution of channel deposits.

Structure-from-motion multi-view stereo (SfM-MVS) photogrammetry makes it possible to provide high-resolution topographic data at low cost compared with conventional topographical surveys (Westoby et al. 2012; James and Robson 2012; Fonstad et al. 2013; Stumpf et al. 2015). In particular, unmanned aerial vehicle-based SfM-MVS photogrammetry (UAV-SfM) can lead to improvements in geomorphic observation because it is immune to surface obstructions and inaccessibility due to complex topography and structures (Westoby et al. 2015; Saito et al. 2018). UAV-SfM has the potential to improve the spatiotemporal resolution of topographic measurement in headwater channels, but its accuracy in such areas has not been thoroughly examined.

UAV-SfM can provide a DEM with a resolution and accuracy of less than a few decimeters if suitable georeferencing is used based on accurate ground control points (GCPs) (De Haas et al. 2014). Differences in coordinates among time series DEMs focusing on the same site hinge on the GCP locations and the measurement accuracy of their coordinates when only GCPs are used for georeferencing (Clapuyt et al. 2016). Consequently, the setting of GCPs is an important factor for the accurate detection of time series differences in elevation resulting from sediment erosion and deposition, but the locations of GCPs in headwater channels are restricted to the vicinity of the channel bed because of steep and inaccessible surface conditions in the hillslope sections. Moreover, DEMs acquired via UAV-SfM include not only rotation errors arising from aerial photographs but also scale errors relating to the uncertainty of georeferencing (Carbonneau and Dietrich 2017). These lead to spatial differences in measurement accuracy between measurement periods. Consequently, topical validations using point data, such as elevation measured by global navigation satellite system (GNSS), are not sufficient, and spatial validations of UAV-SfM are necessary. However, previous topographic data, such as DEMs acquired via ALS, cannot be used for such validations because of frequent fluctuations in sediment storage. Therefore, the accuracy of UAV-SfM in headwater channels has not yet been fully examined.

With this in mind, the accuracy of UAV-SfM in a headwater channel was investigated, based on a comparison of topographic data acquired via UAV-SfM and terrestrial laser scanning (TLS) during a similar measurement period. Using a comparison of the DEMs, we validated the reproducibility of complex topography via UAV-SfM photogrammetry. Moreover, the applicability of point cloud registration using the iterative closest point (ICP) algorithm was examined with a view to increasing the volume estimation accuracy of channel deposits. On the basis of these results, we discuss the applicability of UAV-SfM for topographic measurements in headwater channels.

Methods

Study site

Our study site was located at the upper Ichinosawa torrent of the Ohya landslide in the Southern Japanese Alps (Fig. 1a, b). The Ohya landslide was initiated by an earthquake in 1707, with an estimated total sediment volume of 120 million m^3 (Tsuchiya and Imaizumi 2010). The prominent geological feature in the area is Paleogene strata, which are comprised of highly fractured shale and well-jointed sandstone, and the annual precipitation is approximately 3400 mm (Imaizumi et al. 2016).

The Ichinosawa torrent is located at the northern end of the Ohya landslide. The highest point is 1905 m above sea level (a.s.l.), while the lowest point is a waterfall, located at 1450 m a.s.l. The total length of the channel is approximately 650 m, the average channel inclination is approximately 27°, and the drainage area is 0.22 km^2

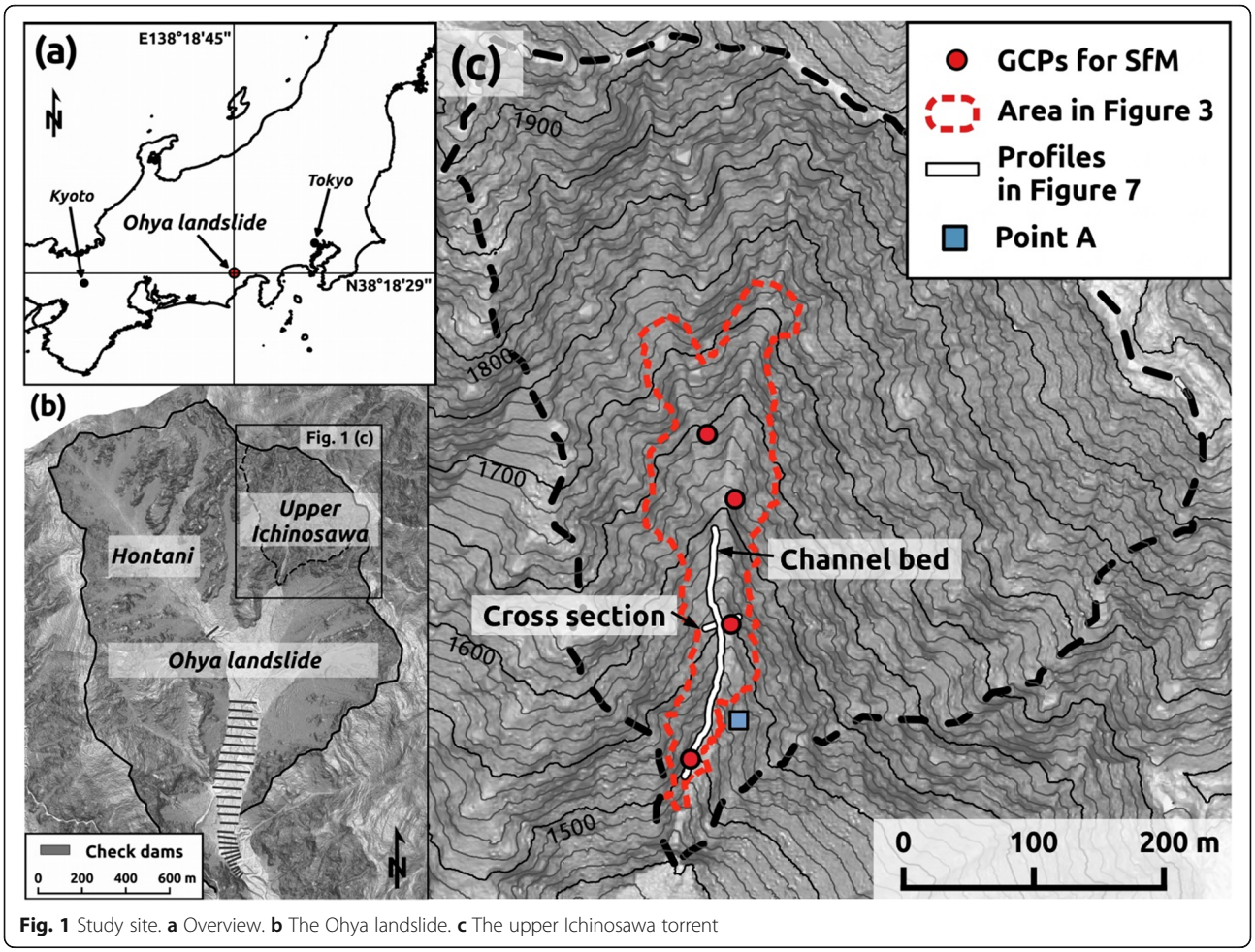

Fig. 1 Study site. **a** Overview. **b** The Ohya landslide. **c** The upper Ichinosawa torrent

(Fig. 1c). The vast majority of the slopes in the upper parts of the hillslopes exceed 38°. During the winter season (December–March), sediment moves from the hillslope to the channel bed via freeze–thaw processes, which promote dry ravel and rock-fall (Fig. 2a) (Imaizumi et al. 2006). In the summer season (June–September), channel deposits are discharged as debris flows during storm events (Fig. 2b). Debris flows occur approximately three or four times per year in this area (Imaizumi et al. 2017, 2019). This area is one of the most active debris flow torrents in Japan. Although sparse vegetation covers part of the hillslopes during the summer–fall season (Fig. 2b), the percentage coverage and vegetative height are less than 30% and 10 m, respectively.

UAV-SfM measurements

We carried out UAV-SfM photogrammetry and TLS during similar periods (September 4 and 5, 2016) in the study site. In nearly all cases, it is expected that the accuracy of a DEM acquired via laser scanning will be higher than that acquired via SfM-MVS photogrammetry (e.g., James and Robson 2012). Therefore, we assumed that the topographic data acquired via TLS was more accurate.

A UAV (DJI Phantom4) was used for the flight on September 4, 2016, covering the channel bed of the upper Ichinosawa torrent (Fig. 1c). In 2016, a total of three debris flow events were observed by monitoring cameras from May to August (Imaizumi et al. 2019). Consequently, the topography of this area in the measurement period consisted of various surface slopes suitable for validating the reproducibility of complex topography.

The weight of the UAV including its battery and propellers was 1380 g, the diagonal size excluding the propellers was 350 mm, the max flight time was approximately 28 min, and a three-axes (pitch, roll, and yaw) gimbal control camera was installed on the bottom of its body. The digital camera sensor (CMOS) size was 1/2.3″, the effective pixel size was 12.4 megapixels, the field of view was 94 degrees 20 mm (35 mm format equivalent), the F measure was 2.8, and the focus was at infinity.

The flight was conducted manually at elevations between 50 m and 200 m above the channel bed. The flight path accounted for an overlap in the photographs of at least 70% to produce an accurate point cloud. We primarily focused on a comparison of the channel deposits

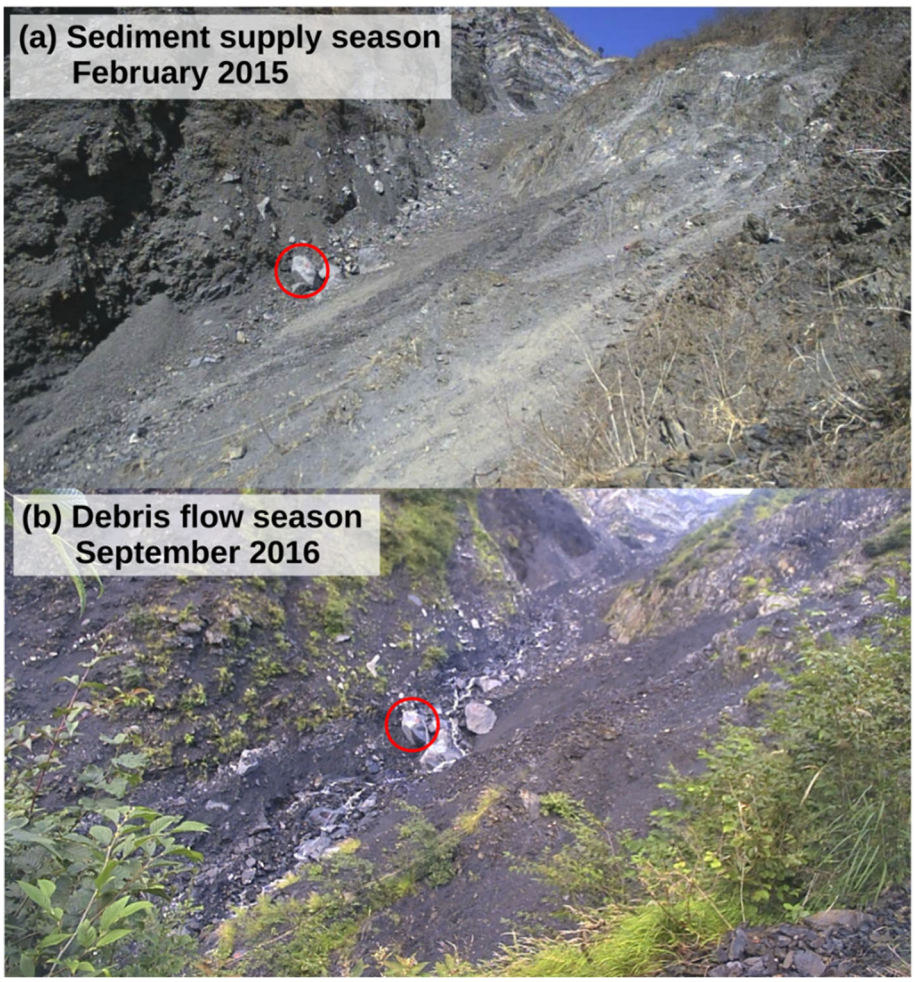

Fig. 2 Photos of channel deposits taken at point A in Fig. 1c during (**a**) the sediment supply season (February 19, 2015) and (**b**) the debris flow season (September 10, 2016). The red circle indicates a large boulder (approximately 2 m) located at the same position in both photos

rather than the hillslopes; accordingly, nearly all the photographs were taken from the vertical direction for the channel bed. Because the weather conditions were cloudy, the amounts of shade, and spatial variations in the brightness were slight in the obtained photographs.

The photographs were processed using the SfM-MVS photogrammetry software (Agisoft PhotoScan Professional), which can produce accurate DEMs if suitable photographs and GCPs are used, for example, it has been used for debris flow fans (De Haas et al. 2014), forest canopies (Jensen and Mathews 2016), and landslide areas (Saito et al. 2018). In the first step of processing, the shooting camera positions for all acquisition photographs (approximately 300 photographs) were detected using the exchangeable image file format data of each photograph. Consequently, the estimated errors of the relative camera positions for each photograph were detected (the average value of the relative estimated errors was 1.262 m), and photographs with estimated errors exceeding 2 m were removed. This process reduced the number of photographs to approximately 170, and the average value of the relative estimated errors decreased to approximately 0.6 m. Following the standard SfM-MVS photogrammetry workflow, a point cloud comprising over 50 million points was produced (see Table 1 for properties of the point cloud).

The georeferencing of the point cloud was conducted using four GCPs (Fig. 1c), and the geographic coordinates of the GCPs were measured using a GNSS receiver (Hemisphere A325). The GCPs were dispersed in domains with fewer undulations (e.g., without large boulders and vegetation) because the reproducibility of SfM-MVS is known to decrease at the boundary of a characteristic surface, such as a structure (James and Robson 2014). The root-mean-square deviation (RMS) of the GNSS measurement for the GCPs ranged from 0.005 to 0.033 m (Table 2). The serial number of the GCPs indicates the order of the GCPs from upper to lower in Fig. 1c. After georeferencing and eliminating points of

Table 1 Point cloud properties acquired via UAV-SfM and TLS

Measurement type	UAV-SfM	TLS
Point density (pt/m^2)	483.6	281.1
Standard deviation in point density (pt/m^2)	112.6	173.2
Average point spacing (mm)	45.5	59.6
Marge of scans	Tie point matching	—
Precision of marge (mm)	<6	—
Interpolator creating DEM	TIN	TIN

uncertainty and noise, the point cloud consisted of approximately 37 million points and the average projection error of the GCPs was approximately 0.004 m. From this point cloud, a DEM (DEM_{SfM}) and orthophotograph were produced, with spatial resolutions of 0.1 m and 0.015 m, respectively. Triangulated irregular network (TIN) interpolation was used to create the DEM (Table 1).

Terrestrial laser scanning

We obtained point cloud data on September 4 and 5, 2016, via TLS to validate the accuracy of the results acquired via UAV-SfM (Table 1). Two TLS units (Topcon GLS-1500 and GLS-2000) were used. The maximum measurable ranges of the scanners were 500 m (for a target object with a 90% reflectance), with distance accuracies of 4 mm (GLS-1500) and 3.5 mm (GLS-2000), respectively, at a range of 150 m and angle accuracies of 6″. A total of five point-cloud data was acquired. A total of eight reference targets were installed and used for the registration of the point cloud data via a target matching (tie-point) method, with accuracies of 0.5–6 mm. Two targets were used for the georeferencing and geographic coordinates as measured by GNSS receivers (Trimble GeoExplorer 6000XH). The overall errors of the registered point cloud, including scanning, registration, and georeferencing, were considered to be on the order of centimeters (Hayakawa et al. 2016). After eliminating noise, a DEM with a 0.1 m resolution (DEM_{TLS}) was produced from the point cloud using TIN interpolation.

Point cloud registration

The alignment of point clouds using the ICP algorithm has been applied to reduce the deviation in the registration error between point clouds acquired via TLS (Teza et al. 2007; Schürch et al. 2011; Hayakawa et al. 2017, Obanawa and Hayakawa 2018). The point cloud acquired via UAV-SfM contains rotation errors (Carbonneau and Dietrich 2017), but it is possible that an ICP-based alignment could decrease such errors. We therefore examined the effectiveness of ICP-based alignment for topographic measurements via UAV-SfM in the headwater channel.

Table 2 Accuracies and RMS of the GCPs used for the georeferencing of UAV-SfM

GCPs	Accuracy x (m)	Accuracy y (m)	Accuracy z (m)	RMS (m)
GCP1	0.007	0.010	0.018	0.032
GCP2	0.005	0.006	0.012	0.031
GCP3	0.008	0.010	0.019	0.010
GCP4	0.012	0.013	0.033	0.029

The ICP algorithm fits a point cloud to a reference point cloud using a transformation matrix (Besl and McKay 1992; Bergevin et al. 1996). The transformation matrix is iteratively computed as a matrix that minimizes the distance between the nearest points on key features of two-point clouds based on similar morphological features in the overlapping area. The hillslope section of a point cloud acquired via TLS was set as the reference point cloud because the hillslope morphology is relatively stable during the summer season. We calculated the transformation matrix and aligned the point cloud acquired via UAV-SfM to fit the reference point cloud using the CloudCompare software (Girardeau-Moutaut et al. 2005). After ICP-based alignment, $DEM_{SfM\text{-}ICP}$ was generated via TIN interpolation, and the resolution was set to 0.1 m.

DEM comparison

We computed the DEMs of the differences (DoD) between DEM_{TLS} and DEM_{SfM} or $DEM_{SfM\text{-}ICP}$ to validate the accuracy of UAV-SfM. $DoD_{TLS\ -\ SfM}$ was calculated by subtracting DEM_{SfM} from DEM_{TLS}. $DoD_{TLS\ -\ SfM\text{-}ICP}$ was calculated by subtracting $DEM_{SfM\text{-}ICP}$ from DEM_{TLS}. To investigate the efficacy of ICP-based alignment, volumetric differences were calculated with respect to the positive and negative domains of $DoD_{TLS\ -\ SfM}$ and $DoD_{TLS\ -\ SfM\text{-}ICP}$ using the equation below, similar to Staley et al. (2014):

$$\Delta V = \frac{A_V \times \sum_{(i,j)=1}^{n} \Delta Z_{(i,j)}}{n}, \quad (1)$$

where A_v is the area of the volume being calculated in m^2 (i.e., total area of positive or negative domains), $\Delta Z_{(i,j)}$ is the change in elevation at each pixel (i,j; given coordinates of each pixel in meter), and n is the total number of pixels in A_v (Staley et al. 2014). The calculated volumetric differences were compared with already-known erosion volume in sediment storage resulting from debris flow, referring to the time series TLS survey by Hayakawa et al. (2016). To investigate the representability of the topography, we compared the spatial distribution and a histogram of the surface slope for each DEM. For the comparison of the spatial distribution of the surface slope, the slope domains were divided into three domains based on the balance between the shear strength

and the shear stress, similar to Imaizumi et al. (2017): saturated sediment (< 21°), unsaturated sediment (21–38°), and bedrock (> 38°, the angle of static friction).

The comparison area was restricted to the vicinity of the channel deposits (Fig. 3c) for the following three reasons: (1) the accuracy around the edge of a DEM produced via SfM-MVS is generally low because of distortion (Carbonneau and Dietrich 2017), (2) the vegetation on the hillslope section causes topical differences in the elevation of DEM_{SfM} compared with the actual topographic surface, and (3) DEM_{TLS} does not sufficiently cover the upper part of the hillslopes because the reflected density of the radiated laser on the upper part of the hillslopes is relatively low. Accordingly, we cannot investigate the accuracy of UAV-SfM including the ridge surrounding the headwater channel. However, nearly all of the topographic changes induced by fluctuations in the sediment storage are induced in the vicinity of the channel (e.g., Imaizumi et al. 2006; Berger et al. 2011a). Therefore, the comparison area is reasonable to validate and discuss the measurement accuracy for sediment storage in headwater channels.

Results and discussion

Figure 3 shows the orthophotograph acquired via UAV-SfM and the DoDs between DEM_{TLS} and DEM_{SfM} or $DEM_{SfM\text{-}ICP}$. While both DoDs indicated a spatial variation in the elevation differences (Fig. 3b, c), the DoDs around the edges of the DEMs exceeded 2 m. $DoD_{TLS - SfM}$ in part of the right bank and channel bed exceeded 0.1 m (Fig. 3b), whereas the domain where the DoD exceeded 0.1 m was relatively small for $DoD_{TLS - SfM\text{-}ICP}$ (Fig. 3c). From the comparison between the DoDs and the orthophotograph, we see that domains with

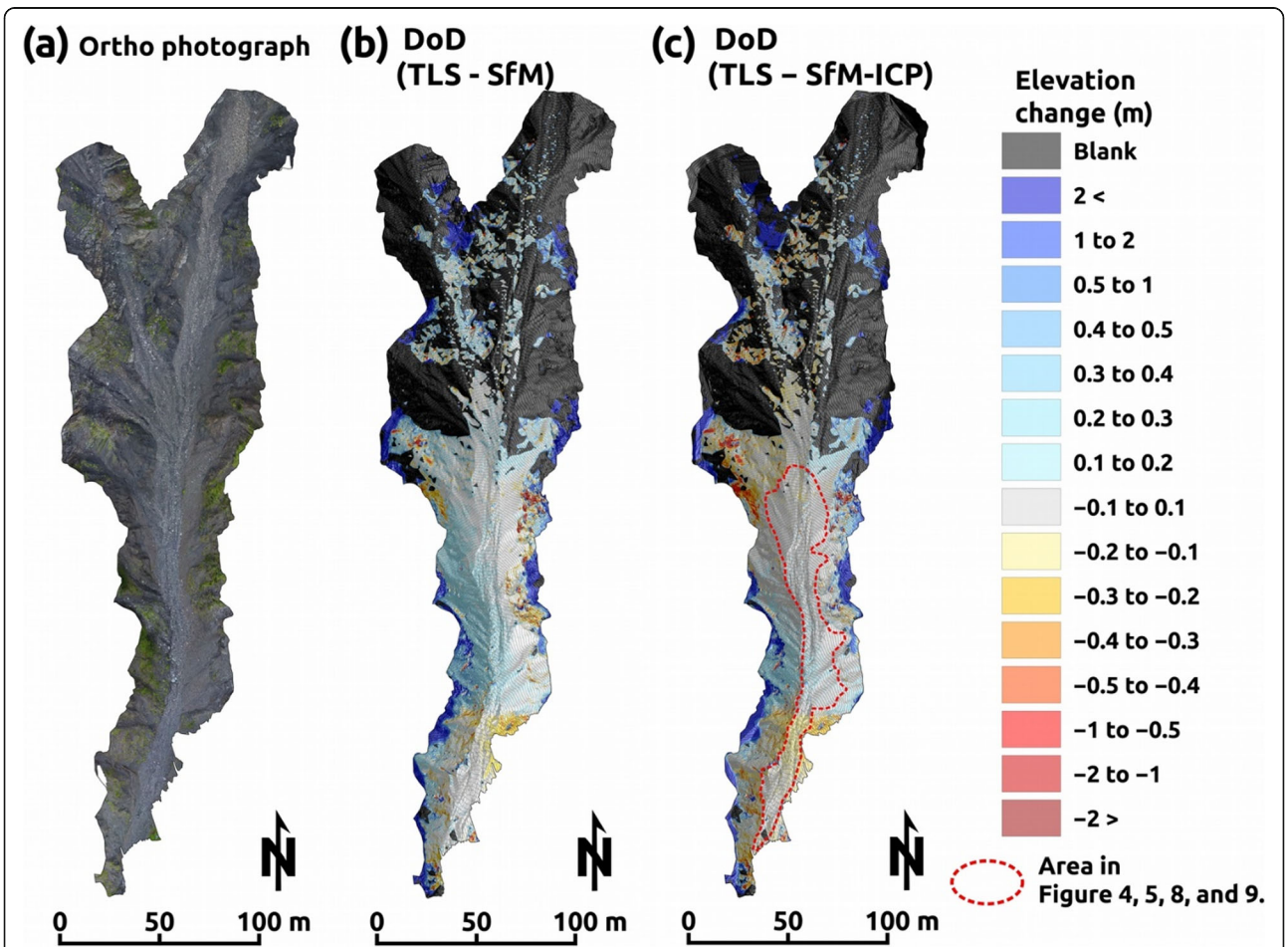

Fig. 3 Results of the UAV-SfM measurements. **a** Orthophotograph of the entire observation area and DEMs of the differences (DoD). **b** Between DEM_{TLS} and DEM_{SfM}. **c** Between DEM_{TLS} and $DEM_{SfM\text{-}ICP}$. Because both DoDs were computed such that DEM_{SfM} or $DEM_{SfM\text{-}ICP}$ was subtracted from DEM_{TLS}, the cold (positive value) and warm (negative value) colors indicate domains where the elevations of DEM_{SfM} or $DEM_{SfM\text{-}ICP}$ are relatively high and low compared to DEM_{TLS}, respectively. The TLS measurement focused on the downstream side of the initiation zone; therefore, there are blank domains indicated by the black color on the upstream side. The domain surrounded by the dotted red line indicates the area used for the validation

substantial DoDs exceeding ± 2 m correspond to domains covered by vegetation (Fig. 3).

Figure 4 shows histograms for the DoDs in the vicinity of the channel bed (the domain surrounded by the red dotted line in Fig. 3c). Nearly all DoDs were within ± 0.4 m. For $DoD_{TLS - SfM}$ (Fig. 4a), the median was 0.06 m and, therefore, the elevation of the UAV-SfM photogrammetry was relatively low compared to that of TLS. After the ICP-based alignment (Fig. 4b), because the deviation in the DoDs was reduced, the median decreased to −0.002 m.

The difference in volume based on the DoDs varied between DEM_{SfM} and $DEM_{SfM\text{-}ICP}$ (Fig. 5). For $DoD_{TLS - SfM}$, the positive difference in volume exceeded 200 m^3, whereas the negative difference was less than 30 m^3. Conversely, the positive and negative differences in volume for $DoD_{TLS - SfM\text{-}ICP}$ were similar at 100 m^3. As a consequence of ICP-based alignment, the net difference in volume (i.e., the absolute value of the sum of the positive and negative values of volumetric differences) was reduced to 6.9 m^3 (Fig. 6). This was low compared with the net difference in volume with respect to DEM_{SfM}

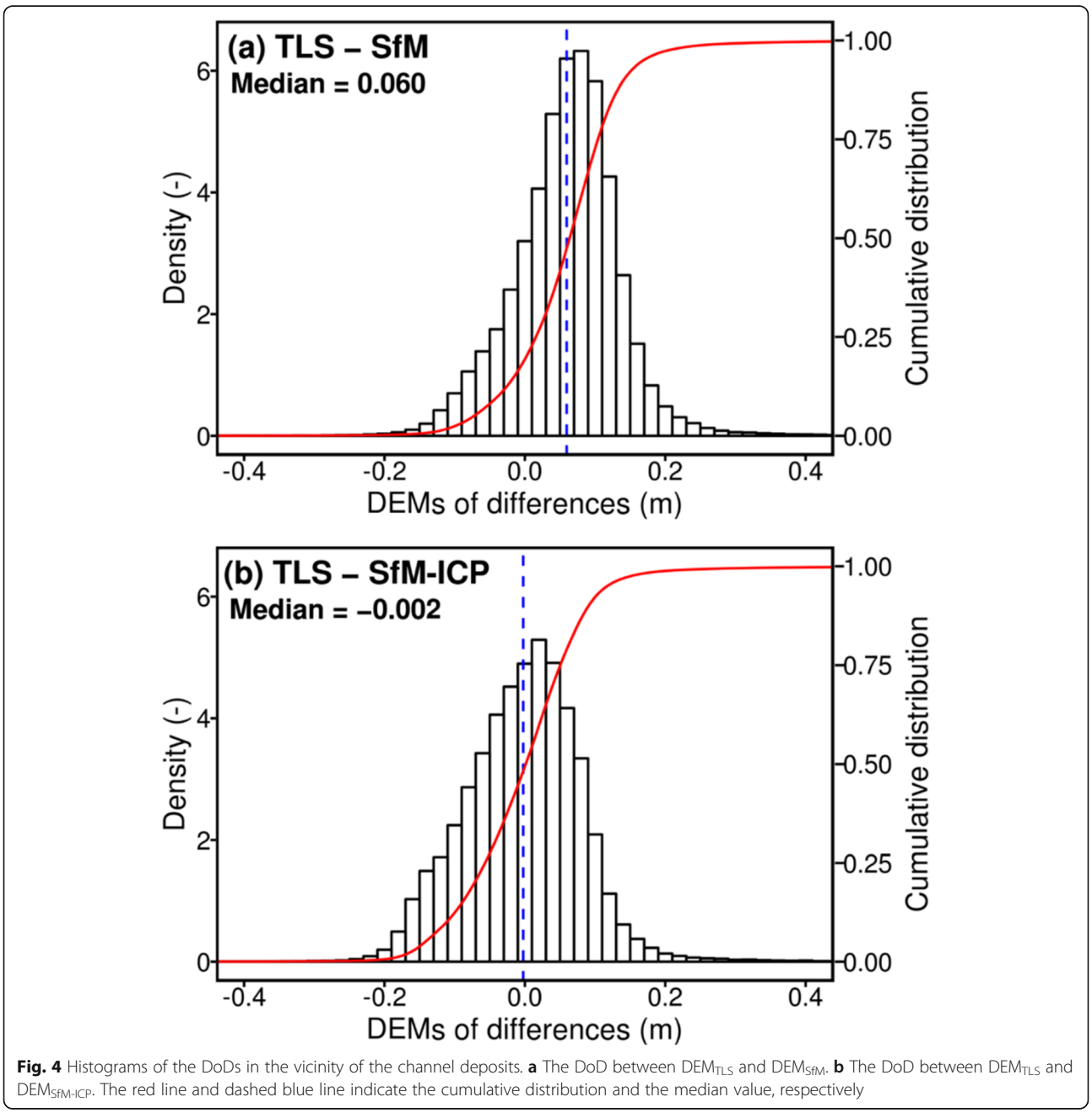

Fig. 4 Histograms of the DoDs in the vicinity of the channel deposits. **a** The DoD between DEM_{TLS} and DEM_{SfM}. **b** The DoD between DEM_{TLS} and $DEM_{SfM\text{-}ICP}$. The red line and dashed blue line indicate the cumulative distribution and the median value, respectively

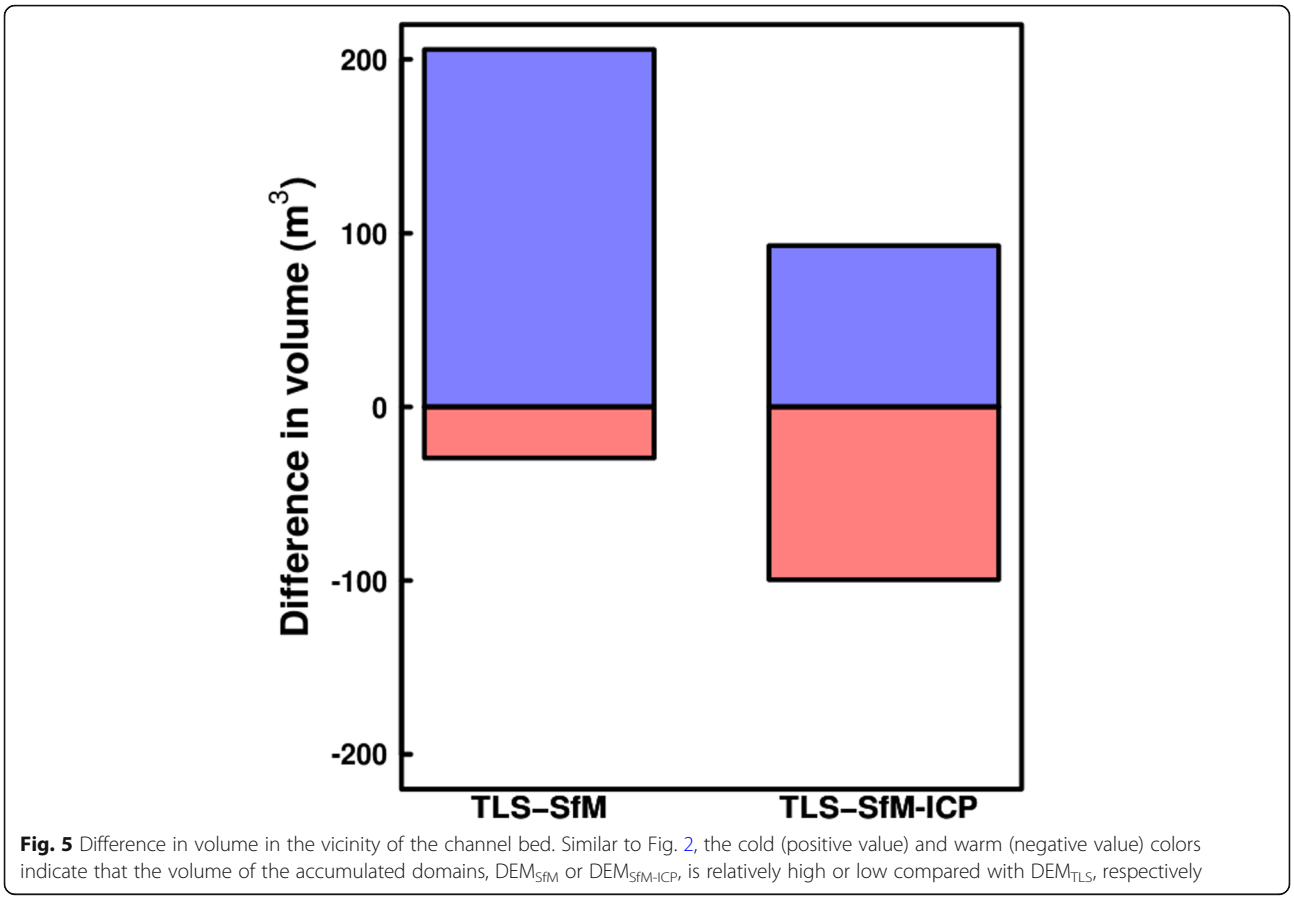

Fig. 5 Difference in volume in the vicinity of the channel bed. Similar to Fig. 2, the cold (positive value) and warm (negative value) colors indicate that the volume of the accumulated domains, DEM_{SfM} or $DEM_{SfM\text{-}ICP}$, is relatively high or low compared with DEM_{TLS}, respectively

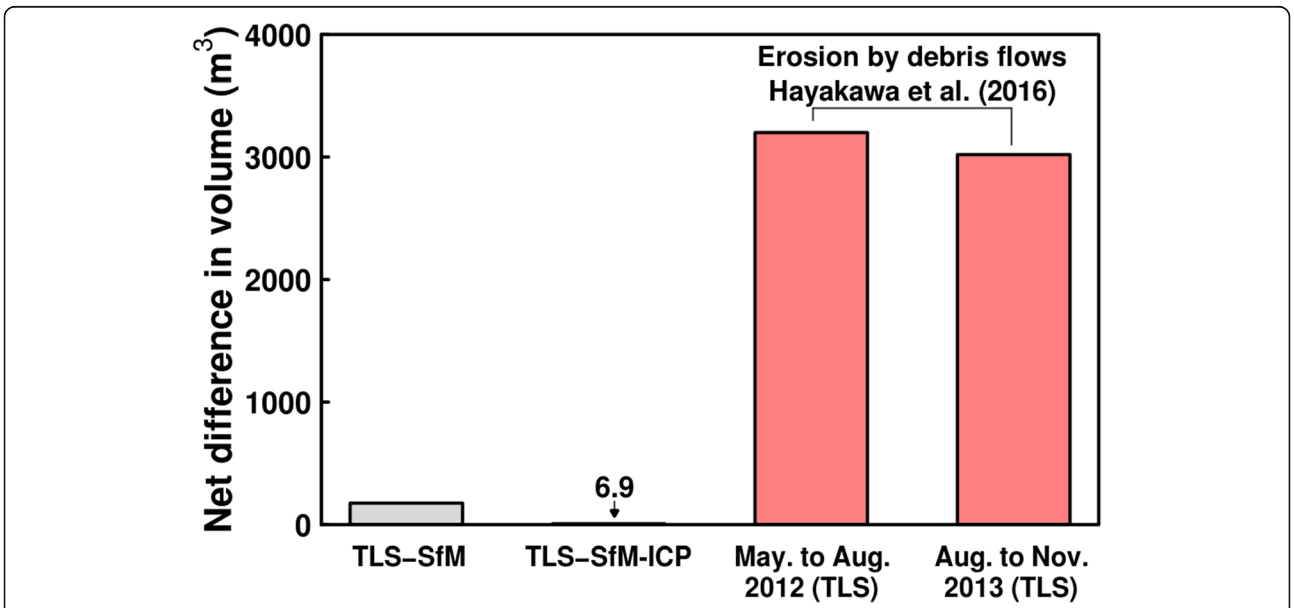

Fig. 6 Difference in net volume in the vicinity of the channel bed. The left two bars indicate the net difference in the volume of DEM_{SfM} or $DEM_{SfM\text{-}ICP}$ versus DEM_{TLS} (i.e., the absolute value of the sum of positive and negative volume in Fig. 5). The right two bars indicate the volume of eroded sediment due to debris flows in our study site investigated by Hayakawa et al. (2016)

(approximately 180 m^3). Moreover, during two different periods, May–August 2012 and August–November 2013, two debris flows occurred, and their eroded volume was approximately 3000 m^3 by TLS measurement (Hayakawa et al. 2016). Considering this, the net difference in volume using UAV-SfM was obviously low compared with the volumetric changes caused by debris flows.

The profiles of the channel bed were similar for the two DEMs because the DoDs along the channel were mostly less than ± 0.2 m (Fig. 7a). Regardless of location, $DoD_{TLS - SfM}$ tended to be high compared with $DoD_{TLS - SfM\text{-}ICP}$. After ICP-based alignment, the spatial trends of the DoDs were similar, and the DoDs approached zero in the channel bed section. Both DoDs in part of the area around 1100–1120 m downward were as much as 0.8 m, which was confirmed to correspond with topical depressions in the channel deposits, using the orthophotograph.

Because nearly all the DoDs of the cross section were also within ± 0.2 m, the profiles of the DEMs were similar (Fig. 7b). On the right bank, $DoD_{TLS - SfM}$ tended to be larger than $DoD_{TLS - SfM\text{-}ICP}$. After ICP-based alignment, the DoDs on the right bank were close to zero, resulting in a decrease in the DoDs around the channel bed. The DoDs in parts of the right and left banks were greater than those around the channel bed, probably due to steep hillslopes. However, the vast majority of the DoDs corresponded to the change point in the profile shape (inclination), e.g., at locations 20–45 m from the right bank.

From the viewpoint of differences in surface type, the spatial distribution of the slope domains was similar for the DEMs (Fig. 8). Moreover, histograms of the slope computed from the DEMs show the similarity in slope distribution (Fig. 9), indicating that the medians were similar, at approximately 35°. The surface topography included steep sections exceeding 38° (the angle of static friction for sediment particles, Imaizumi et al. 2017), but the density of such steep areas was similar for the two DEMs.

Accuracy of topographic data acquired via UAV-SfM

The comparison of the DoDs around the channel demonstrates that all elevation differences between DEM_{SfM} and DEM_{TLS} varied between about −0.4 and 0.4 m (Fig. 4). In addition, the spatial distributions and histograms of the slope calculated using each DEM were similar (Figs. 8 and 9). Therefore, in the vicinity of the channel bed in the headwater channel, the representability of complex topography with UAV-SfM photogrammetry is comparable to that with TLS.

Because DEMs acquired via TLS generally include registration errors resulting from the uncertainty of georeferencing and point matching, the true value of the topography on the order of centimeters is unknown (Obanawa and Hayakawa 2018). However, because the representative grain size of observed debris flows at this site is approximately 0.1–0.3 m (Imaizumi et al. 2016), topographic changes caused by flows nearly always exceed values on the order of decimeters (Hayakawa et al. 2016). The accuracy of DEM_{SfM} is therefore sufficient to detect the entrainment and deposition of channel deposits induced by debris flows. Considering that it has been reported that the grain size of debris flows is over 0.1 m in various debris flow torrents (e.g., Berti et al. 1999; McArdell et al. 2007), UAV-SfM may be able to accurately detect changes in the sediment storage caused by debris flows in many headwater channels.

A relatively large DoD (approximately 0.8 m) was topically detected around a small hole in the channel bed (Fig. 7a), probably due to the limitation of the TLS footprint. Undulations on the surface often behave as obstructions and occlusions in response to scanning positions (Schürch et al. 2011). In this respect, shaded areas result in domains without measured points in the point cloud. This lack of points is generally interpolated based on the elevation of the surrounding points when the point cloud is converted to a DEM. Considering this, the large DoD around the hole may result from inadequate interpolation arising from a lack of measurement points by TLS. This suggests that in some cases, UAV-SfM photogrammetry may surpass TLS for the detection of microtopography in headwater channels.

Estimation of volume changes and effectiveness of the ICP alignment

Considering the steep slope of hillslopes (Figs. 8 and 9), topical differences in elevation may lead to over- or under-estimation regarding channel deposits. As the elevations of DEM_{SfM} in part of the right bank and channel bed were low compared with those of DEM_{TLS} (Fig. 3b), the positive difference in volume was greater than the negative difference (Fig. 5). As shown in Fig. 3b, the DEM acquired via UAV-SfM includes spatial heterogeneous DoDs due to topical distorted shapes caused by the location and accuracy of the GCPs, camera shooting directions, surface structures, and environmental conditions such as solar radiation and shade (James and Robson 2014). In other words, the DEM acquired by UAV-SfM includes more or less uncertain measurement accuracy. However, when considering that the erosion volumes of channel deposits resulting from debris flows obviously exceeded the differences in volume between DEM_{SfM} and DEM_{TLS} (Fig. 6), the measurement accuracy of UAV-SfM is presumably adequate to investigate changes in sediment storage in response to a single debris flow event.

By contrast, the analysis via multi-time series DEM acquired by UAV-SfM should be noted in terms of the accumulation of differences arising from topical

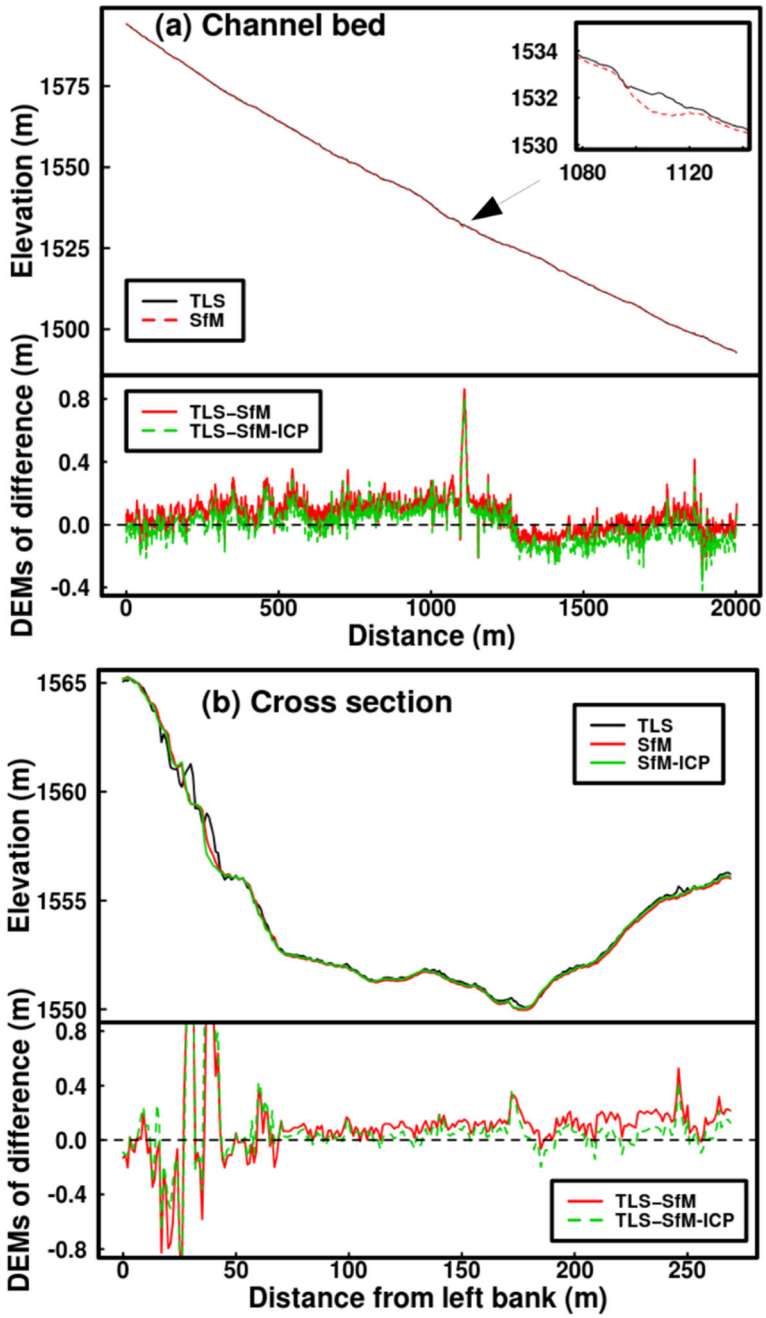

Fig. 7 Comparison of the elevation and DoDs along (**a**) a profile of the channel bed and (**b**) a cross section through the channel, as indicated in Fig. 1. The inset of (**a**) indicates the topical depressions of channel deposits

distortions. The topography of a channel bed is spatially altered because of sediment discharge and recharge (Blasone et al. 2014; Imaizumi et al. 2017). Hence, even though we distributed four GCPs in the area (Fig. 1c), the GCPs were compelled to shift to other stable positions in response to topographic changes. This makes it impossible to control the spatial distribution and coordinate accuracy (e.g., the GNSS measurement) of the GCPs, despite the condition of the GCPs being one of the key factors for the reproducibility of UAV-SfM photogrammetry (Clapuyt et al. 2016). Because of the unavoidable uncertainty arising from the technical limitations of UAV-SfM and the difference in measurement accuracy of GCPs, the spatial distribution of such distortion will be different for each measurement date. These topical differences in elevation are accumulated via the integration of the sediment volumes calculated from the time series DEMs acquired via UAV-SfM. Therefore,

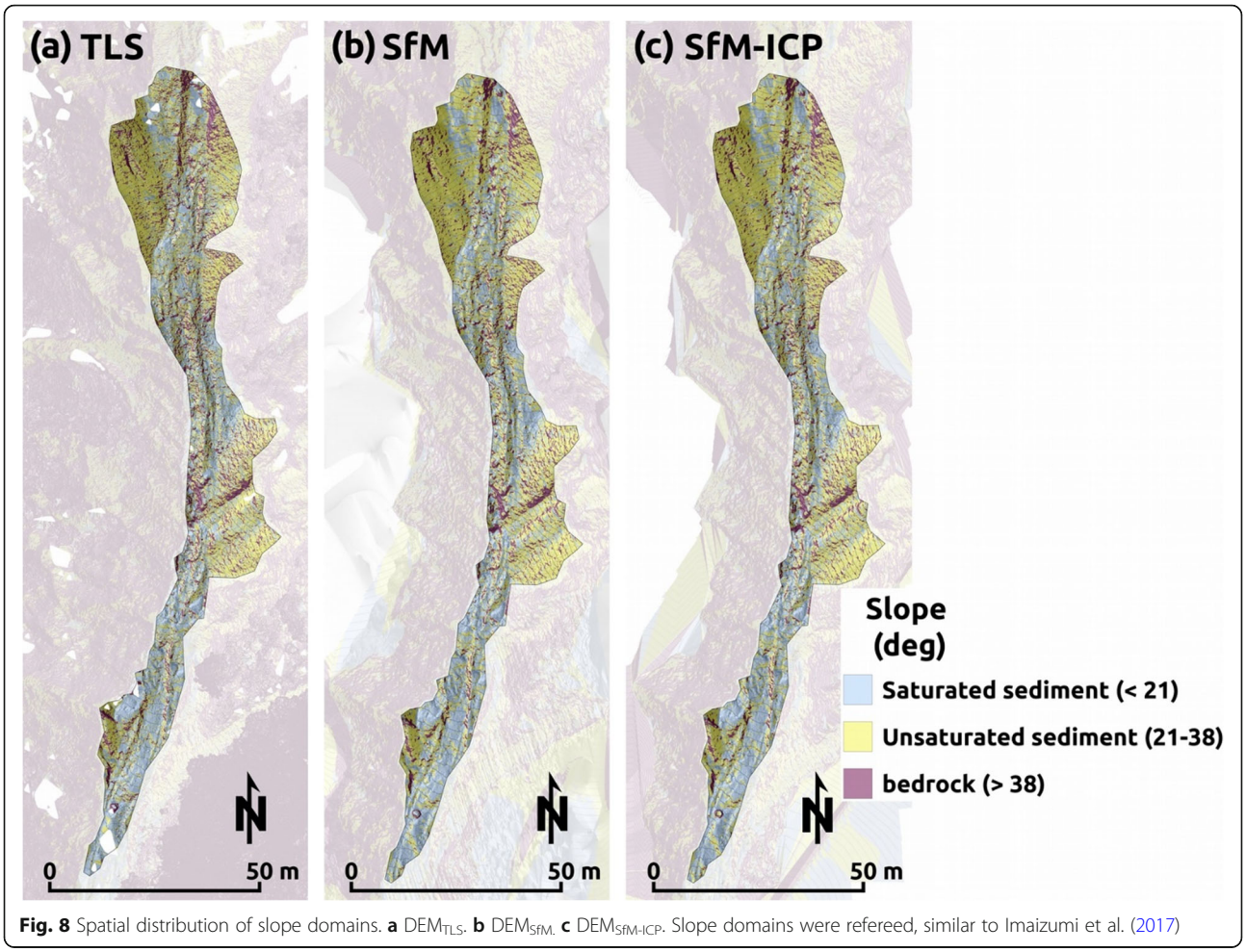

Fig. 8 Spatial distribution of slope domains. **a** DEM_{TLS}. **b** DEM_{SfM}. **c** $DEM_{SfM\text{-}ICP}$. Slope domains were refereed, similar to Imaizumi et al. (2017)

there is a risk of over- or under-estimation or ostensible offset of changes in sediment storage when time series DEMs acquired via UAV-SfM are used.

Domains with DoDs exceeding 0.1 m in part of the right bank and channel decreased after ICP-based alignment (Fig. 3b, c). Therefore, the median of the DoDs in the vicinity of the channel tended toward zero (Fig. 4), and consequently, the difference in the estimated volume between the negative and positive values was smaller compared with the DoDs excluding the ICP-based alignment (Fig. 5). When considering that the DoDs on the right bank significantly decreased after ICP-based alignment (Fig. 7b), these results indicate that this alignment could decrease the topical distortion caused by SfM-MVS. The hillslope topography in the vicinity of the channel bed was relatively unchanged over a long period, suggesting that ICP-based alignment using hillslope topography acquired via previous TLS measurements would alleviate the accumulation of errors such as topical distortions. Therefore, an ICP-based alignment using stable topography acquired via TLS could be an effective process for investigating long-term changes in sediment storage in a headwater channel based on UAV-SfM.

Conclusions

The accuracy of a DEM acquired via UAV-SfM for complex topography in a headwater channel was validated using a DEM and point cloud acquired via TLS. The results indicate that nearly all of the differences in the measured elevation between UAV-SfM and TLS were within ± 0.4 m, with a median of 0.06 m. Therefore, the shapes of the profiles acquired via UAV-SfM were similar to those acquired via TLS. Moreover, the spatial distributions and medians of the surface slope were similar. For the differences in volume calculated by subtracting the DEM acquired via UAV-SfM from that acquired via TLS, the positive difference was 200 m^3, and the negative difference was −30 m^3 because part of the elevation acquired via UAV-SfM was low compared with that acquired via TLS. After ICP-based alignment of the point cloud acquired via UAV-SfM using a reference (TLS) point cloud for the hillslope sections, the median of the differences in elevation decreased to −0.002 m.

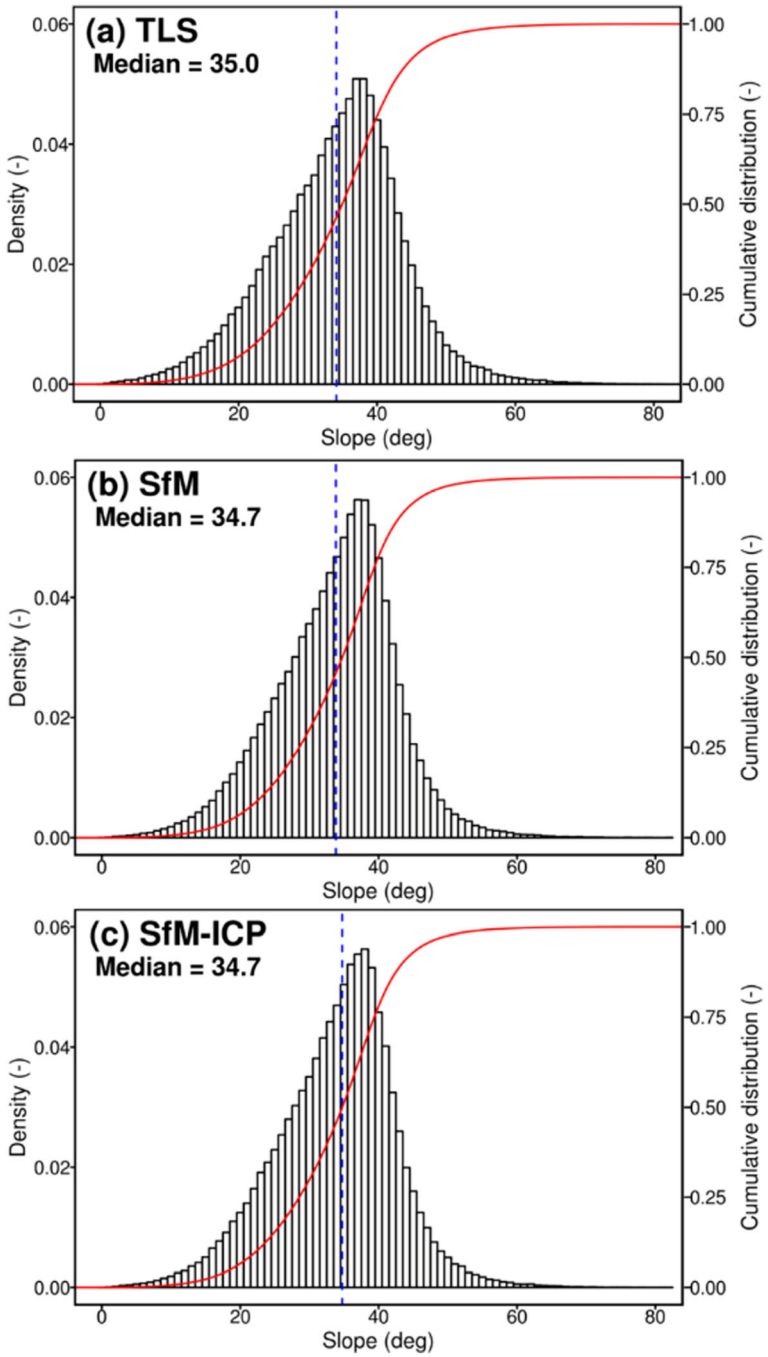

Fig. 9 Histograms of the surface slope in the vicinity of the channel deposits. **a** DEM_{TLS}. **b** DEM_{SfM}. **c** $DEM_{SfM\text{-}ICP}$. Similar to Fig. 4, the red line and dashed blue line indicate the cumulative distribution and the median value, respectively

Consequently, the deviation of the estimated volume was reduced, resulting in both positive and negative differences of approximately 100 m^3. This demonstrates that the accuracy of DEMs acquired via UAV-SfM is comparable with those acquired via TLS and that ICP-based alignment using point clouds acquired via TLS is effective for the accurate estimation of time series volumetric changes with respect to channel deposits.

Abbreviations

ALS: Airborne laser scanning; GCP: Ground control point; GNSS: Global navigation satellite system; ICP: Iterative closest point; RMS: Root-mean-square deviation; SfM-MVS: Structure from motion multi-view-stereo;

TIN: Triangulated irregular network; TLS: Terrestrial laser scanning; UAV: Unmanned aerial vehicle

Acknowledgements
The authors are grateful to Takeshi Masui, Yushi Yokota, Yuichi Sakai, and the students at Shizuoka University for their assistance in the field observations.

Authors' contributions
HT conducted field measurements using an UAV and data analysis, and drafted this manuscript. NH collaborated with the corresponding author in the construction of the manuscript. YSH carried out TLS measurements in the field and data analysis. FI helped field measurements. All authors read and approved the final manuscript.

Funding
This work was supported by JSPS KAKENHI grant numbers 16 J02197, 18 J01961, and 25702014.

Availability of data and materials
The data used in this paper are available from the authors on request.

Competing interests
The authors declare that they have no competing interests.

Author details
[1]Forestry and Forest Products Research Institute, 1, Matsunosato, Tsukuba, Ibaraki 305-8687, Japan. [2]Faculty of Agriculture, The University of Tokyo, 1-1-1, Yayoi, Bunkyo-ku, Tokyo 113-8657, Japan. [3]Faculty of Environmental Earth Science, Hokkaido University, N10W5, Sapporo, Hokkaido 060-0810, Japan. [4]Faculty of Agriculture, Shizuoka University, 836, Ohya, Suruga-ku, Shizuoka 422-8529, Japan.

Received: 5 December 2019 Accepted: 18 May 2020
Published online: 08 June 2020

References

Bel C, Liébault F, Navratil O, Eckert N, Bellot H, Fontaine F, Laigle D (2017) Rainfall control of debris-flow triggering in the Réal Torrent, Southern French Prealps. Geomorphology 291:17–32
Berger C, McArdell BW, Schlunegger F (2011a) Direct measurement of channel erosion by debris flows, Illgraben, Switzerland. J Geophys Res Earth Surf 116: F01002. https://doi.org/10.1029/2010JF001722
Berger C, Schlunegger F, McArdell BW (2011b) Sediment transfer patterns at the Illgraben catchment, Switzerland: implication for the time scales of debris flow activities. Geomorphology 125:421–432
Bergevin R, Marc S, Gagnon H, Laurendeau D (1996) Towards a general multi-view registration technique. IEEE Trans Pattern Anal Mach Intell 18(5):540–547
Berti M, Genevois R, Simoni A, Tecca PR (1999) Field observations of a debris flow event in the Dolomites. Geomorphology 29:265–274
Besl PJ, McKay ND (1992) A method for registration of 3-D shapes. IEEE Trans Pattern Anal Mach Intell 14(2):239–256
Blasone G, Cavalli M, Marchi L, Cazorzi F (2014) Monitoring sediment source areas in a debris-flow catchment using terrestrial laser scanning. Catena 123:23–36
Carbonneau PE, Dietrich JT (2017) Cost-effective non-metric photogrammetry from consumer-grade sUAS: implications for direct georeferencing of structure from motion photogrammetry. Earth Surf Process Landf 42:473–486
Clapuyt F, Vanacker V, Oost KV (2016) Reproducibility of UAV-based earth topography reconstructions based on structure-from-motion algorisms. Geomorphology 260:4–15
Coe JA, Kinner DA, Godt JW (2008) Initiation conditions for debris flows generated by runoff at Chalk Cliffs, central Colorado. Geomorphology 96: 270–297
De Haas T, Ventra D, Carbonneau PE, Kleinhas MG (2014) Debris-flow dominance of alluvial fans masked by runoff reworking. Geomorphology 217:165–181
Fonstad MA, Dietrich JT, Courville BC, Jensen JL, Carbonneau PE (2013) Topographic structure from motion: a new development in photogrammetric measurement. Earth Surf Process Landf 38(4):755–766
Gallo F, Lavé J (2014) Evolution of a large landslide in the high Himalaya of central Nepal during the last half-century. Geomorphology 223:20–32
Girardeau-Moutaut D, Roux M, Marc R, Thibault G (2005) Change detection on points cloud data acquired with a ground laser scanner. Int Arch Photogrammetry Remote Sensing Spat Inform Sci 36:30–35
Hayakawa YS, Imaizumi F, Hotta N, Tsunetaka H (2016) Towards long-lasting disaster mitigation following a mega-landslide: high-definition topographic measurement of sediment production by debris flows in a steep headwater channel. In: Meadows M, Lin JC (eds) Geomorphology and Society (Advances in Geographical and Environmental Sciences Series). Springer, pp 125–147
Hayakawa YS, Kusumoto S, Matta N (2017) Seismic and inter-seismic ground surface deformation of the Murono mud volcano (central Japan): a laser scanning approach. Prog Earth Planet Sci 4(3). https://doi.org/10.1186/s40645-016-0116-3
Imaizumi F, Hayakawa YS, Hotta N, Tsunetaka H, Ohsaka O, Tsuchiya S (2017) Interaction between the accumulation of sediment storage and debris flow characteristics in a debris-flow initiation zone, Ohya landslide body, Japan. Nat Hazards Earth Syst Sci 17:1923–1938
Imaizumi F, Masui T, Yokota Y, Tsunetaka H, Hayakawa YS, Hotta N (2019) Initiation and runout characteristics of debris flow surges in Ohya landslide scar, Japan. Geomorphology. 339:58–69
Imaizumi F, Nishii R, Murakami W, Daimaru H (2015) Parallel retreat of rock slopes underlain by alternation of strata. Geomorphology 238:27–36
Imaizumi F, Sidle RC, Tsuchiya S, Ohsaka O (2006) Hydrogeomorphic processes in a steep debris flow initiation zone. Geophys Res Lett 33:L10404
Imaizumi F, Tsuchiya S, Ohsaka O (2016) Behavior of boulders within a debris flow initiation zone. Int J Erosion Control Engin 9(3):91–100
James MR, Robson S (2012) Straightforward reconstruction of 3D surfaces and topography with a camera: accuracy and geoscience application. J Geophys Res Earth Surf 117:1–17
James MR, Robson S (2014) Mitigating systematic error in topographic models derived from UAV and ground-based image networks. Earth Surf Process Landf 39:1413–1420
Jensen JL, Mathews AJ (2016) Assessment of image-based point cloud products to generate a bare earth surface and estimate canopy heights in a woodland ecosystem. Remote Sens 8(1):50
McArdell BW, Bartelt P, Kowalski J (2007) Field observations of basal forces and fluid pore pressure in a debris flow. Geophys Res Lett 34:L07406. https://doi.org/10.1029/2006GL029183
McCoy SW, Kean JW, Coe JA, Staley DM, Wasklevicz TA, Tucker GE (2010) Evolution of a natural debris flow: in situ measurements of flow dynamics, video imagery, and terrestrial laser scanning. Geology 38:735–738
McCoy SW, Kean JW, Coe JA, Tucker GE, Staley DM, Wasklevicz TA (2012) Sediment entrainment by debris flows: in situ measurements from the headwaters of a steep catchment. J Geophys Res Earth Surf 117:F03016. https://doi.org/10.1029/2011JF002278
McCoy SW, Tucker GE, Kean JW, Coe JA (2013) Field measurement of basal forces generated by erosive debris flows. J Geophys Res Earth Surf 118:589–602. https://doi.org/10.1002/jgrf.20041
Nishii R, Imaizumi F, Daimaru H, Murakami W (2018) Continuous and large sediment supply in a steep landslide scar, Southern Japanese Alps. Geomorphology 312:51–59
Obanawa H, Hayakawa YS (2018) Variation in volumetric erosion rates of bedrock cliffs on a small inaccessible coastal island determined using measurements by an unmanned aerial vehicle with structure-from-motion and terrestrial laser scanning. Prog Earth Planetary Sci 5(33). https://doi.org/10.1186/s40645-018-0191-8
Saito H, Uchiyama S, Hayakawa YS, Obanawa H (2018) Landslides triggered by an earthquake and heavy rainfalls at Aso Volcano, Japan, detected by UAS and SfM-MVS photogrammetry. Prog Earth Planetary Sci 5(15). https://doi.org/10.1186/s40645-018-0169-6
Schlunegger F, Badoux A, McArdell BW, Gwerder C, Schnydrig D, Rieke-Zapp D, Molnar P (2009) Limits of sediment transfer in an alpine debris-flow catchment, Illgraben, Switzerland. Quat Sci Rev 28:1097–1105
Schürch P, Densmore AL, Rosser NJ, Lim M, McArdell BW (2011) Detection of surface change in complex topography using terrestrial laser scanning: application to the Illgraben debris-flow channel. Earth Surf Process Landf 36: 1847–1859
Staley DM, Wasklewicz TA, Coe JA, Kean JW, SW MC, Tucker GE (2011) Observations of debris flows at Chalk Cliffs, Colorado, USA: Part 2, changes in surface morphometry from terrestrial laser scanning in the summer of 2009. In: Genevois R, Hamilton DL, Prestininzi A (eds) Proceedings of the Fifth International Conference on Debris Flow Hazards Mitigation/Mechanics,

Prediction, and Assessment, Padua, Italy, June 7-11, 2011. Italian Journal of Engineering Geology and Environment—Book, Casa Editrice Universita La Sapienza, pp 759–768
Staley DN, Wasklewicz TA, Kean JW (2014) Characterizing the primary material sources and dominant erosional processes for post-fire debris-flow initiation in a headwater basin using multi-temporal terrestrial laser scanning data. Geomorphology 214:324–338
Stumpf A, Malet J-P, Allemand P, Pierrot-Doseillingny M, Skupinski G (2015) Ground-based multi-view photogrammetry for the monitoring of landslide deformation and erosion. Geomorphology 231:130–145
Teza G, Galgaro A, Zaltron N, Genevois R (2007) Terrestrial laser scanner to detect landslide displacement fields: a new approach. Int J Remote Sens 28:3425–3446
Tsuchiya S, Imaizumi F (2010) Large sediment movement caused by the catastrophic Ohya-kuzure landslide. J Dis Res 3(5):257–263
Westoby MJ, Brasington J, Glasser NF, Hambrey MJ, Reynolds JM (2012) 'Structure-from-Motion' photogrammetry: a low-cost, effective tool for geoscience applications. Geomorphology 179:300–314
Westoby MJ, Dunning SA, Woodward J, Hein AS, Marrero SM, Sugden DE (2015) Sedimentological characterization of Antarctic moraines using UAVs and structure-from-motion photogrammetry. J Glaciol 61(230):1088–1102

Publisher's Note